Influence of annealing on the distribution of thermoelectric figure of merit in bismuth-telluride ingots

O. YAMASHITA, H. ODAHARA
Faculty of Engineering, Ehime University, Bunkyocho, Matsuyama 790-8577, Japan
E-mail: yamashio@eng.ehime-u.ac.jp; yamashio567@yahooo.co.jp

Published online: 12 January 2006

The *p*-type $(Bi_{0.25}Sb_{0.75})_2Te_3$ doped with 8 wt% excess Te alone and *n*-type $Bi_2(Te_{0.94}Se_{0.06})_3$ codoped with 0.017 wt% Te and 0.068 wt% I were grown by the Bridgman method and were cut into a parallelepiped of $5 \times 5 \times 15$ mm^3, where the length of 15 mm is parallel to the freezing direction. The specimen is mounted on an *X*-*Y* stage and the temperature difference between two probes set at an interval of 1 mm was approximately 2.6 K. The local Seebeck coefficient α_ℓ and local electrical resistivity ρ_ℓ along the freezing direction were measured at a scan step of 1 mm before and after annealing at 673 K for 2 h in vacuum. The local thermal conductivity κ_ℓ was calculated from ρ_ℓ using the relation between κ and ρ obtained previously for a series of bismuth-telluride compounds. As a result, α_ℓ ρ_ℓ and κ_ℓ before and after annealing changed significantly from place to place, so that the effect of annealing on the local thermoelectric figure of merit $(ZT)_\ell$ was never uniform throughout the specimen surface. The maximum $(ZT)_\ell$ of the as-grown *p*- and *n*-type specimens reached surprisingly great values of 1.88 and 1.59 at 298 K, respectively, which correspond to about twice as large as those observed macroscopically by the conventional Seebeck coefficient apparatus with an interval (between two probes) of 8 mm. Probably, these maximum values of $(ZT)_\ell$ would be an upper limit of *ZT* for the *p*- and *n*-type bismuth- telluride bulk compounds, at least in the present fabrication method.

1. Introduction

Bismuth-telluride (Bi_2Te_3) is one of the best thermoelectric materials with the highest figure of merit ($ZT = \alpha^2 T/\rho\kappa$), where α is the Seebeck coefficient, ρ the electrical resistivity, κ the thermal conductivity and T the absolute temperature [1]. A larger figure of merit Z directly leads to higher conversion efficiency. Whereas much effort has been made to raise Z of bulk materials based on Bi_2Te_3 by doping or alloying other elements in various fabricating processes, *ZT* has not been much improved and is not much more than 1. By annealing the ingots prepared by the Bridgman method, however, we have most recently achieved high *ZT* of 1.19 at 298 K for the *n*-type $Bi_2(Te_{0.94}Se_{0.06})_3$ alloy [2] and 1.41 at 308 K for the *p*-type $(Bi_{0.25}Sb_{0.75})_2Te_3$ alloy [3], so that both *ZT* were able to exceed 1.

As conventional fabricating techniques of bismuth-telluride bulk compounds, there are melting techniques due to Bridgman [4], Czochralski [5] and zone-melting [6] methods and powder metallurgy techniques such as hot-pressing [7, 8] and hot-extrusion [9] methods. The specimens prepared by these methods were often subjected to the annealing in various atmospheres to raise *ZT* as high as possible [2, 7]. However, the annealing has either a favorable effect or an adverse effect on the improvement in *ZT* of bismuth-telluride bulk compounds [2–5, 7]. This is merely the macroscopic annealing effect all over the specimen volume. As a matter of course, it is expected that *ZT* before and after annealing may vary microscopically from place to place. From this reason, we attempted to visualize the distribution of the local thermoelectric figure of merit $(ZT)_\ell$ before and after annealing. The local Seebeck coefficient α_ℓ and local electrical resistivity ρ_ℓ before and after annealing were measured at every position on the surface of a specimen. The local thermal conductivity κ_ℓ was estimated as the sum of the local electronic component κ_{el} and local lattice one κ_{lat}; κ_{el} and κ_{lat} were calculated from ρ_ℓ using the Wiedemann-Franz law and the relation between κ_{lat} and ρ, respectively, where the latter relation has been obtained macroscopically for

0022-2461
DOI: 10.1007/s10853-005-2209-z

a series of bismuth-telluride compounds which have the same principal chemical composition as those of the specimens used here and are subjected to the same fabrication method [10]. The mapping of α_ℓ ρ_ℓ andκ_ℓ over the specimen surface yields a lot of information and is essential for materials researches on complex and multi-compositional systems. Therefore, it is of importance to investigate what effect the annealing has on the local thermoelectric properties.

Fifteen years ago, the technology of the nanoscale lateral mapping of electrical resistivity [11] and chemical potential [12] has been developed mainly by Wickramasinghe *et al*. using a forced thermal gradient between a probe and the specimen surface, in which the variation in the chemical potential is directly connected to the Seebeck coefficient. This work was the first attempt to visualize the distribution of Seebeck coefficient. Shortly afterward, this technique has been applied by Ivanova *et al*. [13] to the mapping of the Seebeck coefficient of bismuth-telluride single-crystals grown by the Bridgman method, in order to investigate the change in the distribution of Seebeck coefficient before and annealing. However, their measurement was limited to the Seebeck coefficient alone. Up to now, similar measurements of α_ℓ also have been carried out by some researchers [14–16].

Recently, there have been some theoretical predictions [17–19] that the thermoelectric devices composed of superlattices will eventually have extremely high *ZT* as compared with those of the corresponding bulk materials due to the effects of the quantum confinement of carriers. Indeed, the dramatic increase in *ZT* has been observed in the *p*-type Bi_2Te_3/Sb_2Te_3 and *n*-type $Bi_2Te_3/Bi_2Te_{2.83}Se_{0.17}$ superlattice devices [20], in which their *ZT* reached extremely great values of 2.4 and 1.4 at 300 K, respectively, but such high *ZT* has not yet been realized in bulk materials. However, the application of superlattice devices is limited to small cooling systems such as a pinpoint cooling. Therefore, the appearance of bulk thermoelectrics with higher *ZT* is strongly desired because they are available for any application.

The purpose of this study is to investigate to what extent α_ℓ ρ_ℓ and κ_ℓ before and after annealing of bismuth-telluride polycrystalline ingots vary from place to place and to what extent the maximum value of the resultant local thermoelectric figure of merit $(ZT)_\ell (= \alpha_\ell^2 T/\kappa_\ell \rho_\ell)$ approaches *ZT* values of superlattice devices, resulting in the revelation of an upper limit of *ZT* for the bismuth-telluride bulk materials.

2. Experiments

The *p*-type $(Bi_{0.25}Sb_{0.75})_2Te_3$ doped with 8 wt% excess Te alone and *n*-type $Bi_2(Te_{0.94}Se_{0.06})_3$ codoped with 0.017 wt% Te and 0.068 wt% I (see Table I) were prepared by the Bridgman method, using purer Bi granules of 99.999% and pure Sb, Te, Se and I of 99.99% as starting materials. The materials were weighed out in appropriate atomic ratios, charged into a quartz tube and melted in an evacuated quartz tube by an induction heating to make a homogeneous melt without segregation. After melting, the compounds were unidirectionally solidified by the Bridgman method at a fast rate of 6 cm/h, to produce intentionally second-phase precipitates scattered in an ingot. It is the same growth rate as that employed in preparing the previous specimens [2, 3] and is close to one of various growth conditions reported by Yim and Rosi [4]. Naturally, the resulting ingots were not single crystals and consisted of relatively coarse grains with the cleavage planes (*c* plane) aligned parallel to the freezing direction.

TABLE I Additional content of additives to the *p*-type $(Bi_{0.25}Sb_{0.75})_2Te_3$ and *n*-type $Bi_2(Te_{0.94}Se_{0.06})_3$ specimens

		Additional content (wt%)	
Sample no.	Type	Te	I
1	*p*	8.00	–
2	*n*	0.017	0.068

In order to investigate the thermoelectric properties of the ingots, they were cut into a parallelepiped of $5 \times 5 \times 15$ mm^3 and a square plate of $10 \times 10 \times 3$ mm^3 from the central part of ingots with a total length of about 20 cm, where the length of 15 mm and the thickness of 3 mm was cut parallel to the freezing direction. The former specimens were subjected to Seebeck coefficient and electrical resistivity measurements (Sinku-Riko, Inc., Model ZEM-1), and the latter ones to thermal conductivity after cutting into a disk of $\varphi 10 \times 3$ mm. The Seebeck coefficient α, electrical resistivity ρ and thermal conductivity κ before and after annealing at 673 K for 2 h in vacuum were measured at 298 K within an accuracy of 1, 2 and 2%, respectively. The Seebeck coefficient measurement was made using two alumel-chromel thermocouples set at an interval of 8 mm, with the temperature difference of about 5 K. The resultant accuracy was about 5% as a thermoelectric figure of merit. These macroscopic experimental results are listed in Table I.

However, commercially available apparatus is insufficient to measure the Seebeck coefficient in the local region (within a few mm), because it is not allowed to change arbitrarily the interval between two thermocouples. From this reason, we designed and made an apparatus that is capable of measuring the local Seebeck coefficient α_l in the local region as small as 1 mm in distance. Fig. 1 shows a schematic of the apparatus. It has two alumel-chromel thermocouples (0.25 mm in diameter) to detect temperatures and an electric voltage on a specimen surface, where thermocouples are set at an interval of 1 mm. The specimen is mounted on an *X-Y* stage and the temperature gradient was applied with two Peltier modules equipped to both ends of the specimen. The measurement of α_ℓ was made by producing the temperature difference of about 40 K between both ends of a specimen along the freezing direction; one end of a specimen was heated and another

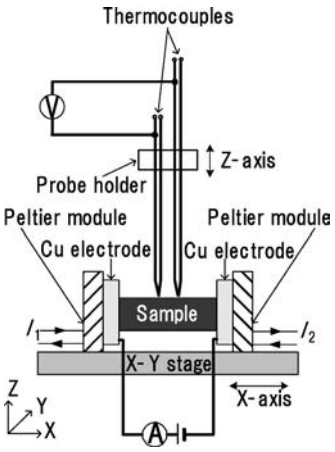

Figure 1 Schematic configuration for measurements of the local Seebeck coefficient α_ℓ and local electrical resistivity ρ_ℓ. One end was heated by flowing the electrical current I_1 or I_2 through a Peltier module to produce the temperature differences and another one was then maintained at room temperature. Two alumel-chromel thermocouples of this apparatus were set at an interval of 1 mm.

end was maintained at 285 K by flowing the electrical current I_1 or I_2 through a Peltier module ($20 \times 20 \times 3$ mm^3). The temperature difference ΔT between two probes put on a specimen surface was then approximately 2.6 K and it was measured with an accuracy of 0.1 K. α_ℓ was estimated using the relation $\alpha_\ell = \Delta V/\Delta T$ with an accuracy of 4% or less, where ΔV is a voltage appeared on two probes. The local electrical resistivity ρ_ℓ was measured at 298 K along the freezing direction by the four-probe method. The measurements of α_ℓ and ρ_ℓ were made on the specimen surface at a scan step of 1 mm along the direction parallel to the heat flux. During these measurements, two probes were put on the specimen by a constant pressure of 0.5 N, so that they contact tightly with the specimen surface.

As well-known, $\sigma\,(=1/\rho)$ and κ of the bismuth-telluride compounds have a strong anisotropy, that is, $\sigma_\perp$ and $\kappa_\perp$ are 2–3 times larger than $\sigma_\parallel$ and $\kappa_\parallel$, respectively, independently of the conduction type, where the symbols $\perp$ and $\parallel$ denote directions perpendicular and parallel to the c axis, respectively [21]. However, there is little crystallographic anisotropy in α [21]. The local difference in the degree of alignment of the c plane of bismuth-telluride compounds, therefore, may be reflected directly in ρ_ℓ and κ_ℓ but little in α_ℓ For this reason, XRD measurement was made before and after annealing on the cross-section (5×5 mm^2) perpendicular to the freezing direction using Cu-Kα radiation, in order to investigate whether the degree of alignment of the c plane changes with the annealing. In addition, XRD measurement was also made before and after annealing on the specimen surface used for α_ℓ and ρ_ℓ measurements, in order to observe whether the precipitated phases such as islands or lamellae have the same crystal structure as that of the alloy matrix.

3. Results and discussion

3.1. Characterization of *p*-type $(Bi_{0.25}Sb_{0.75})_2Te_3$ and *n*-type $Bi_2(Te_{0.94}Se_{0.06})_3$ specimens

XRD measurement was made before and after annealing on the total surface (5×15 mm^2) parallel to the freezing direction of the *p*-type $(Bi_{0.25}Sb_{0.75})_2Te_3$ and *n*-type $Bi_2(Te_{0.94}Se_{0.06})_3$ specimens, whose surface is used for later α_ℓ and ρ_ℓ measurements. As shown in Fig. 2, however, no extra peak except for Bragg peak from rhombohedral type crystal structure was detected before and after annealing at 673 K for 2 h in vacuum, although islands or lamellae appear clearly on their specimen surfaces, as shown in Figs 4a and 7a. The size of such islands and lamellae was little changed by the annealing, as shown in their figures.

Next, the degree of alignment of the cleavage planes (c plane) parallel to the freezing direction of the ingot was investigated before and after annealing on the cross-section (5×5 mm^2) perpendicular to the freezing direction, as shown in Fig. 2. As evident from the fact that the intensity ratio of (0 0 6) to (0 1 5) peak was very small and was almost the same in both *p*- and *n*-type specimens, the cleavage planes of most of grains are found to be parallel to the freezing direction. Moreover, XRD patterns were little changed before and after annealing, so that it was proved that the crystallographic direction of grains is little changed by the annealing.

The chemical compositions and microstructures of the *p*-type $(Bi_{0.25}Sb_{0.75})_2Te_3$ doped with excess 8 wt% Te alone and $Bi_2(Te_{0.94}Se_{0.06})_3$ codoped with 0.017 wt% Te and 0.068 wt% I have ever been investigated before and after annealing at 673 K for 2 h in vacuum [2, 3]. That is, the as-grown *p*-type $(Bi_{0.25}Sb_{0.75})_2Te_3$ specimen is a

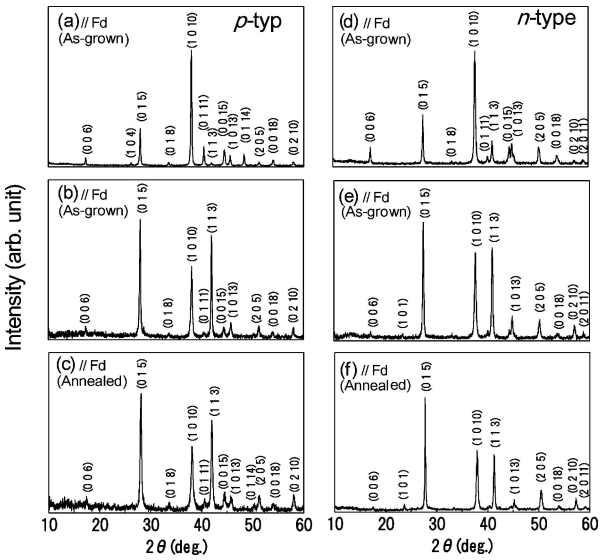

Figure 2 XRD patterns for the cross-sections (5×5 mm) parallel to the freezing direction (Fd) of the as-grown *p*-type, (a) and *n*-type, (d) ingots and perpendicular to the freezing direction of the as-grown *p*-type, (b) and *n*-type,(e) ones and annealed *p*-type, (c) and *n*-type (f) ingots.

two-phase material consisting of an alloy matrix and a second phase. The second phase appears on an etched cross-section as lamellae and islands, which are precipitates of insoluble constituents. The EPMA analysis revealed that the second phase was composed of the Te-rich phase of >90 at% Te, <6 at% Sb and <2 at% Bi and precipitated out along grain boundaries and cleavage planes [2]. After annealing, the second phase of the excess Te was dispersed to some extent, due to the diffusion of Te into the matrix, so that lamellae became thinner. The vacuum annealing at a high temperature of 673 K close to the melting point of the Te-rich phase, promoted somewhat the diffusion of the second phase. On the other hand, the as-grown *n*-type $Bi_2(Te_{0.94}Se_{0.06})_3$ specimen has the Se-rich structure as lamellae. This Se-rich structure was little changed by the annealing. The Se-rich regions just correspond to the Te-poor regions and vice versa, although a constitutive element of Bi showed a homogeneous distribution.

3.2. Dependence of κ on ρ

The dependence of κ on ρ for bismuth-telluride bulk compounds has been reported by the present authors [10]. The chemical compositions of the *p*- and *n*-type specimens used in this experiment were $(Bi_{0.25}Sb_{0.75})_2Te_3$ doped with 3–12 wt% excess Te alone and $Bi_2(Te_{0.94}Se_{0.06})_3$ codoped with 0.017–0.026 wt% Te and 0.068–0.102 wt% I, respectively. Some of the as-grown specimens were annealed, in order to prepare specimens with much different ρ. These polycrystalline specimens have almost the same degree of alignment of the *c* plane parallel to the freezing direction. The electrical rersistivity ρ and thermal conductivity κ were measured at 298 K along the freezing direction and κ was plotted as a function of ρ. In general, κ is expressed as the sum of the lattice thermal conductivity κ_{lat} and the electronic one κ_{el} [1]. Therefore, the lattice component κ_{lat} is obtained by subtracting the electronic component κ_{el} from the observed κ, where κ_{el} was calculated using Wiedemann-Franz law LT/ρ, where L is Lorentz number and T the absolute temperature. As shown in Fig. 3, the dependence of κ on ρ was expressed as a function of ρ for both type specimens; $\kappa = 7.27/\rho + 0.0975\rho - 0.207$ for the *p*-type specimen and $\kappa = 7.27/\rho + 0.0919\rho - 0.043$ for the *n*-type one, where κ and ρ are indicated in units of W/mK and $\mu\Omega$m, respectively [10].

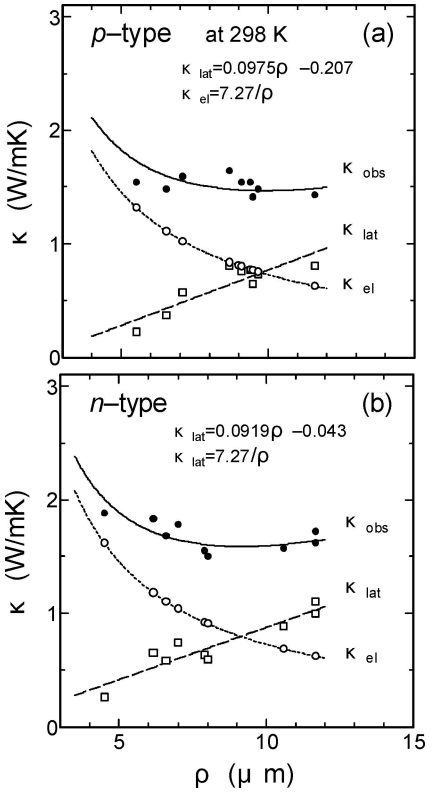

Figure 3 Thermal conductivities κ_{obs}, κ_{el} and κ_{lat} as a function of ρ for the as-grown and annealed *p*-type $(Bi_{0.25}Sb_{0.75})_2Te_3$ (a) and *n*-type $Bi_2(Te_{0.94}Se_{0.06})_3$ (b) specimens.

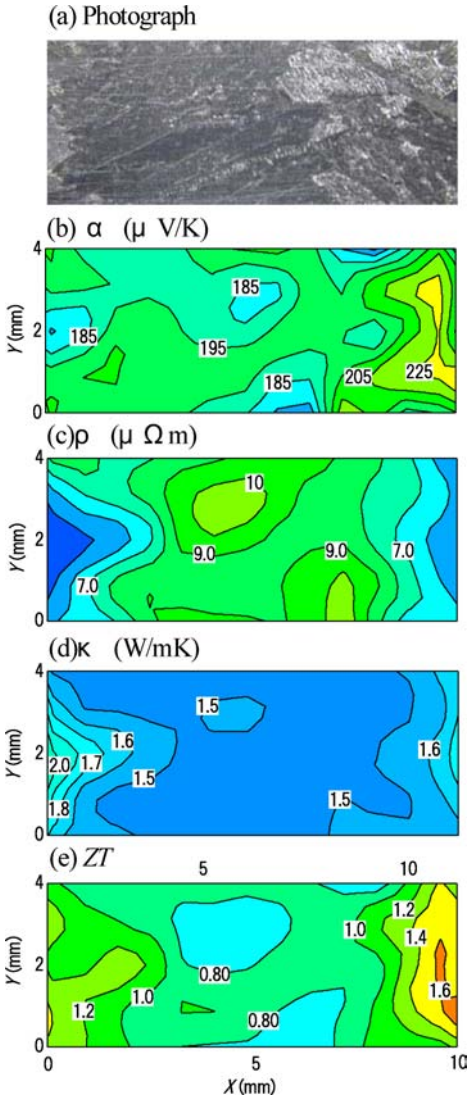

Figure 4 (a) Macroscopic photograph, (b) Local Seebeck coefficient α_ℓ, (c) Local electrical resisitivity ρ_ℓ, (d) Local thermal conductivity κ_ℓ and (e) Local thermoelectric figure of merit $(ZT)_\ell$ mapped as functions of X and Y for the as-grown *p*-type $(Bi_{0.25}Sb_{0.75})_2Te_3$ specimen.

The correlation coefficients between κ_{lat} and ρ for the p- and n-type specimens were 88 and 93%, respectively, so that κ_{lat} was found to be expressed as a linear form of ρ. These relations between ρ and κ should hold even for the local region, because these expressions are obtained for a series of bismuth-telluride compounds which have the same principal chemical composition as those of the specimens used here and are prepared under the same fabrication condition. The local thermal conductivity κ_ℓ values of the p- and n-type specimens were calculated by substituting the observed ρ_ℓ instead of ρ into these two expressions.

3.3. α_ℓ, ρ_ℓ, κ_ℓ and $(ZT)_\ell$ of the p-type specimen before and after annealing

The local electrical resistivity ρ_ℓ of the p-type specimen was measured at 298 K before and after annealing along the freezing direction. The measurement of the local Seebeck coefficient α_ℓ was made by producing the temperature difference of about 40 K between both ends of a specimen along the freezing direction; one end of a specimen was heated to 317 K and another was cooled to 279 K, so that the central part of a specimen is maintained at 298 K. Here ρ_ℓ and α_ℓ measurements were made on the same specimen surface. The substantial length of a specimen used for α_ℓ measurement is 10 mm, and the temperatures of the hot and cold sides of the measured region were 311 and 285 K. The temperature dependence of α of the present p-type specimen is expressed by the relation $\alpha/\alpha_0 = 0.307 \pm 2.33 \times 10^{-3}\, T$ in the region from 280 to 320 K [22] and is little changed before and after annealing [2], where α_0 is the Seebeck coefficient at 298 K. α_ℓ values observed at different temperatures before and after annealing were corrected to the local Seebeck coefficient at 298 K by multiplying α_ℓ by a factor of $(0.307 \pm 2.33 \times 10^{-3}T)^{-1}$. The degree of correction was about 3% at most.

As shown in Figs 4 and 5, ρ_ℓ and the corrected α_ℓ changed significantly from place to place, even when scanned along the y axis (see Fig. 1) on a specimen. This is a notable point, because ρ_ℓ should never change with the scanning along the y axis at least for the constant x, as long as the cross-section (y-z plane of 5×5 mm^2) perpendicular to the freezing direction (x-axis) at each probe position forms an equipotential surface. It indicates that there are a number of local regions with much different ρ along the x axis in a specimen. In other words, it means that the thermoelectric properties near the region lying between two probes are apt to be reflected predominantly in α_ℓ and ρ_ℓ. In order to check the accuracy of the apparatus, the average values of α_ℓ and ρ_ℓ were compared with those observed macroscopically by the conventional Seebeck coefficient apparatus, where they were obtained by averaging over the surface of 10×4 mm^2, not over the total surface of 15×5 mm^2, in order to exclude the end effect. As a whole, these average values of α and ρ before and after annealing were somewhat low compared

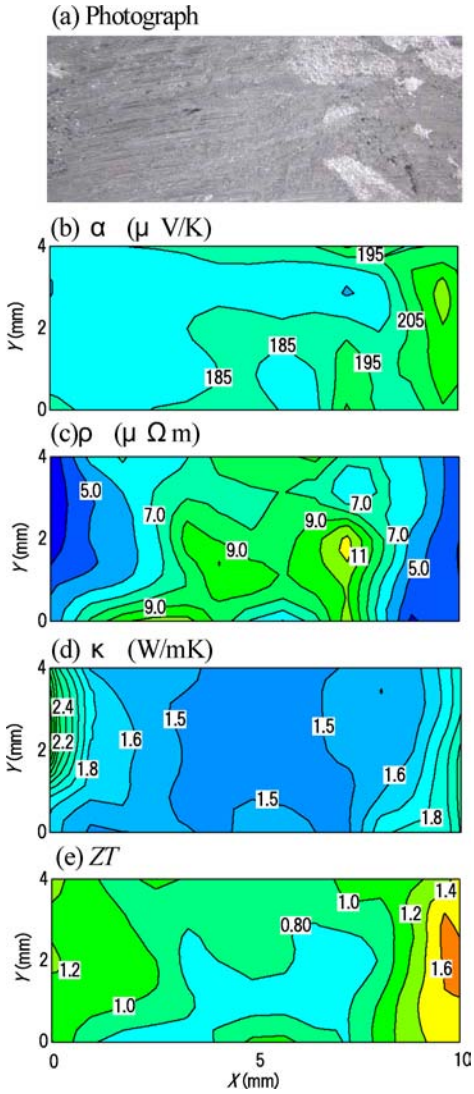

Figure 5 (a) Macroscopic photograph, (b) Local Seebeck coefficient α_ℓ (c) Local electrical resisitivity ρ_ℓ (d) Local thermal conductivity κ_ℓ and (e) Local thermoelectric figure of merit $(ZT)_\ell$ mapped as functions of X and Y for the annealed p-type $(Bi_{0.25}Sb_{0.75})_2Te_3$ specimen, where annealing was done at 673 K for 2 h in vacuum.

to those listed in Table II. This disagreement is considered to be caused by the above reason; one is that the measuring region within a specimen is different from each other and another is that the contribution to ρ_ℓ and α_ℓ from the thermoelectric properties of the local region within the volume ($1 \times 5 \times 5$ mm^3) lying between two probes depends on the position of the local region and is never uniform throughout the volume. In a word, the contribution from the local regions with lower ρ becomes a little larger than that from those with higher ρ, so that the microscopic ρ_ℓ becomes slightly lower than the macroscopic ρ. The same also may hold for α_ℓ. It is considered that the microscopic ρ_ℓ and α_ℓ are affected significantly even by only a slight change in the thermoelectric properties of the local region near the probe, particularly when the interval between two probes is short.

TABLE II Thermoelectric properties measured at 298 K by the conventional method for the as-grown and annealed *p*- and *n*-type bismuth-telluride specimens, where annealing was done at 673 K for 2 h in vacuum

		p-type		*n*-type	
		As-grown	Annealed	As-grown	Annealed
Seebeck coefficient	α (μ V/K)	200	204	−216	−219
Electrical resistivity	ρ (μ Ωm)	9.40	8.35	11.7	9.68
Thermal conductivity	κ (W/mK)	1.54	1.51	1.62	1.60
Figure of merit	ZT	0.82	0.98	0.73	0.92

Figs 4 and 5 show the contour maps of α_ℓ ρ_ℓ and κ_ℓ for the as-grown and annealed *p*-specimens, along with their macroscopic photographs. α_ℓ of the *p*-type specimen has a shaper peak at the right side of a specimen before and after annealing, but the annealing lowered slightly a peak of α_ℓ. Since α_ℓ has little crystallographic anisotropy, however, the significant spatial variation in α_ℓ is considered to result from a very small deviation (∼0.1 wt%) of melt composition in the Te content, as pointed out by Ivanova *et al*. [5]. However, we cannot identify precisely the place where such a deviation from the stoichiometry occurs in a specimen, because the Seebeck coefficients of various places within the volume lying between two probes contribute to α_ℓ. ρ_ℓ before and after annealing has two plateaus around the central part on a specimen surface and takes a low value at both sides of a specimen. As mentioned earlier, since ρ_ℓ has a strong anisotropy, the difference in ρ_ℓ thus may result from only a little change in the degree of alignment of the *c* plane, but we cannot observe it directly, as in the case of α_ℓ. Therefore, it is natural that there is no correlation between the distributions of ρ_ℓ and α_ℓ On the other hand, κ_ℓ has a hollow around the central part on a specimen surface and takes a high value at both sides of a specimen, independently of annealing. A map of κ_ℓ tends to make a pronounced contrast with that of ρ_ℓ. It means that $\kappa_{\rm el}$ is more dominant than $\kappa_{\rm lat}$ in the *p*-type specimen.

As expected, the resultant local figure of merits $(ZT)_\ell$ at 298 K vary significantly from place to place and exhibited a higher value at both sides of a specimen than at its central part, as shown in Figs 4e and 5e. However, the distribution state of $(ZT)_\ell$ was not changed significantly by the annealing. $<ZT>$ was also obtained by the same way as that employed in deriving $<\alpha>$ and $<\rho>$. $<ZT>$ values before and after annealing were 1.07 and 1.05 at 298 K, respectively, which are a little higher than those listed in Table II. This difference between $<ZT>$ and ZT results predominantly from the difference in ρ, as evident from the experimental results listed in Tables II and III. The maximum $(ZT)_\ell$ of the as-grown and annealed *p*-type ingots reached surprisingly great values of 1.88 and 1.68, respectively, which correspond to about twice as large as those observed macroscopically by the conventional Seebeck coefficient apparatus and are the largest among bismuth-telluride bulk compounds. It was thus revealed that there is the local region giving an extremely high ZT even in bismuth-telluride ingots. However, the present maximum $(ZT)_\ell$ is still rather low compared to an extremely high value of ∼2.4 obtained by Venkatasubramanian *et al*. for the *p*-type Bi_2Te_3/Sb_2Te_3 superlattices [20].

α_ℓ ρ_ℓ and κ_ℓ vary before and after annealing, even in the same local region, so that the effect of annealing on $(ZT)_\ell$ of bismuth-telluride bulk ingots was found to be never uniform all over a specimen surface.

3.4. α_ℓ, ρ_ℓ, κ_ℓ and $(ZT)_\ell$ of the *n*-type specimen before and after annealing

α_ℓ and ρ_ℓ measurements of the *n*-type specimen were made in the same manner as the *p*-type specimen. The temperature dependence of α of the present *n*-type specimen is expressed by the relation $\alpha/\alpha_0 = 0.764 \pm 7.96 \times 10^{-4}T$ in the region from 280 to 320 K [22] and is little changed before and after annealing [2], like the *p*-type specimen. α_ℓ values observed at different temperatures before and after annealing were corrected to the local Seebeck coefficient at 298 K by multiplying α_ℓ by a factor of $(0.764 \pm 7.96 \times 10^{-4}T)^{-1}$. The degree of correction of the *n*-type specimen was about 1% at most and smaller than that of the *p*-type specimen. Figs 6 and 7 show the contour maps of α_ℓ ρ_ℓ and κ_ℓ at 298 K before and after annealing. α_ℓ before annealing has a sharp peak at the left side, while after annealing the peak position shifted to the central region. Such a shift seems to have nothing to do with a lamella structure, because the shape of lamellae remains unchanged before and after annealing. When the *n*-type specimen was annealed, the scattering of α_ℓ was increased. Indeed, the standard deviation σ_α of

TABLE III Average values and standard deviations of thermoelectric properties measured at 298 K by a newly fabricated apparatus for the as-grown and annealed *p*- and *n*-type bismuth-telluride specimens, where annealing was done at 673 K for 2 h in vacuum

		p-type		*n*-type	
		As-grown	Annealed	As-grown	Annealed
$<\alpha>$	(μV/K)	198.4	188.6	−203.7	−196.3
σ_α	(μV/K)	15.2	10.7	13.3	27.1
$<\rho>$	($\mu\Omega$m)	8.11	7.27	10.4	8.09
σ_ρ	($\mu\Omega$m)	1.50	1.93	2.20	1.63
$<\kappa>$	(W/mK)	1.58	1.71	1.66	1.72
σ_κ	(W/mK)	0.20	0.41	0.08	0.34
$<ZT>$		1.07	1.05	0.81	0.95
σ_{ZT}		0.31	0.28	0.28	0.29

α_ℓ after annealing was 2.5 times as large as that before annealing, as listed in Table III. It has been reported previously by Teramoto and Takayanagi [23] that α and ρ are very sensitive to the change in the Se content (x) in the $Bi_2(Te_{1-x}Se_x)_3$ alloy system with $x < 0.2$. The high and low α_ℓ in absolute value are thus expected to correspond to the Se-rich and Se-poor regions, respectively, since α_ℓ has little crystallographic anisotropy. Probably, the annealing would cause only a slight change in the Se content, even in the same local region. This may be the reason that α_ℓ is scattered significantly by the annealing. Of course, we cannot identify the place where such segregation occurs in a specimen, as mentioned earlier. ρ_ℓ before annealing has three peaks and two hollows. These peak positions of ρ_ℓ were also shifted significantly by the annealing, but they are away from the peak position of α_ℓ. However, since the degree of alignment of the c plane of the grains is little changed by the annealing, the shift of peak positions of ρ_ℓ may result from only a slight change in the Se content. $<\alpha>$ and $<\rho>$ before and after annealing were somewhat lower in absolute value than those listed in Table II, as in the case of the p-type specimen. A map of κ_ℓ was in contrast with that of ρ_ℓ as in the case of the p-type specimen, but the spatial variation in κ_ℓ of the as-grown and annealed n-type ingots was unexpectedly small compared to that of the p-type ones.

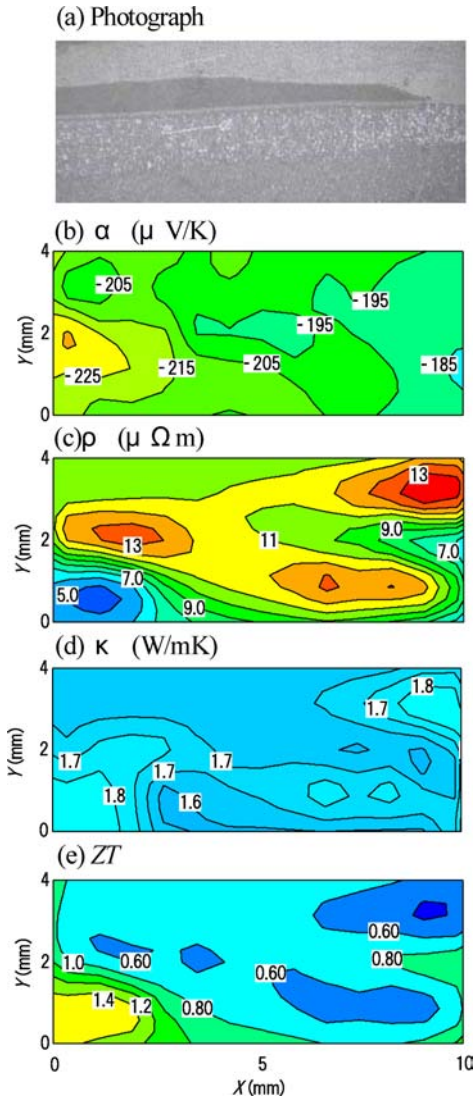

Figure 6 (a) Macroscopic photograph, (b) Local Seebeck coefficient α_ℓ, (c) Local electrical resisitivity ρ_ℓ, (d) Local thermal conductivity κ_ℓ and (e) Local thermoelectric figure of merit $(ZT)_\ell$ mapped as functions of X and Y for the as-grown n-type $Bi_2(Te_{0.94}Se_{0.06})_3$ specimen.

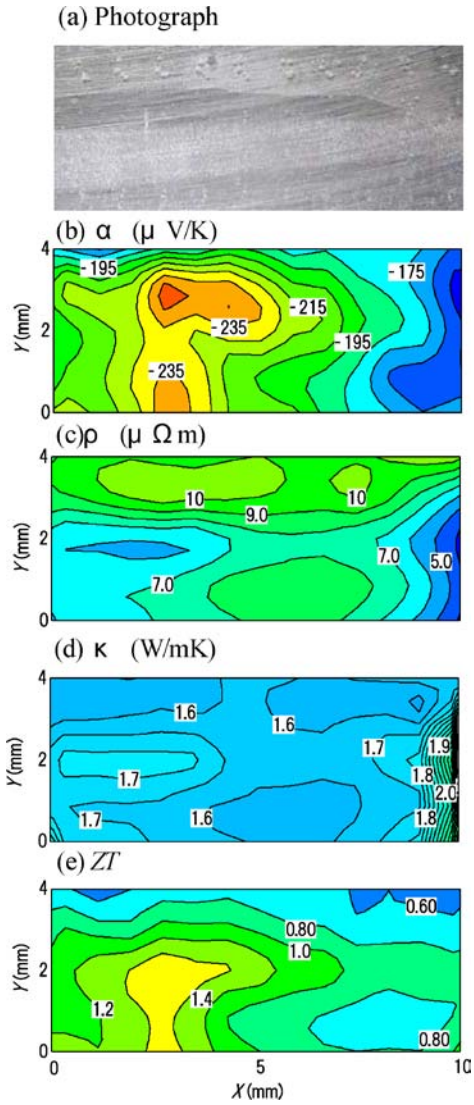

Figure 7 (a) Macroscopic photograph, (b) Local Seebeck coefficient α_ℓ, (c) Local electrical resisitivity ρ_ℓ, (d) Local thermal conductivity κ_ℓ and (e) Local thermoelectric figure of merit $(ZT)_\ell$ mapped as functions of X and Y for the annealed n-type $Bi_2(Te_{0.94}Se_{0.06})_3$ specimen, where annealing was done at 673 K for 2 h in vacuum.

As shown in Figs 6e and 7e, the distribution of $(ZT)_\ell$ at 298 K varied significantly before and after annealing, unlike the p-type specimen. The effect of annealing on the improvement in $(ZT)_\ell$ of bismuth-telluride bulk ingots depends strongly on the local position and was never uniform throughout the specimen, like the p-type specimens. $<ZT>$ values before and after annealing were 0.81 and 0.95, respectively, which are a little higher than the macroscopic ZT values listed in Table II, respectively. The degree of agreement between $<ZT>$ and ZT of the n-type

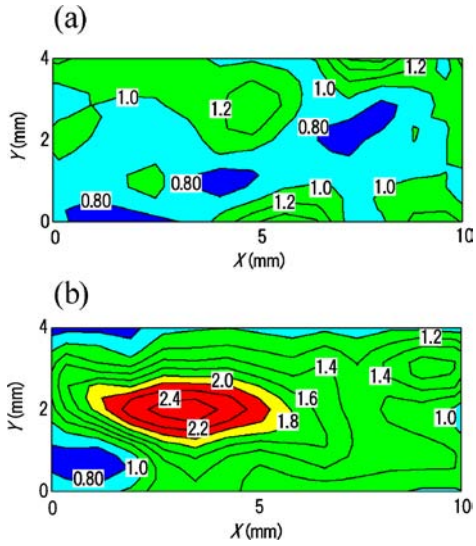

Figure 8 $(ZT)^a_\ell/(ZT)^b_\ell$ mapped as functions of *X* and *Y* for the *p*-type (a) and *n*-type (b) specimens, where $(ZT)^a_\ell$ and $(ZT)^b_\ell$ are the local thermoelectric figure of merits after and before annealing, respectively.

specimen is considerably better than that of the *p*-type one. The maximum $(ZT)_\ell$ of the as-grown and annealed *n*-type ingots also reached great values of 1.59 and 1.55, respectively, which are rather low compared to those of the *p*-type specimens, but surprisingly are a little higher than 1.4 obtained by Venkatasubramanian *et al*. for the *n*-type $Bi_2Te_3/Bi_2Te_{2.83}Se_{0.17}$ superlattice devices [20]. This indicates that there is the local region fitted better to the enhancement in *ZT* even in bulk materials and it is possible to obtain an extremely high *ZT* without making superlattice structures.

Probably, the present maximum $(ZT)_\ell$ values of the *p*- and *n*-type ingots would be an upper limit of *ZT* for the *p*- and *n*-type bismuth-telluride bulk compounds, at least in the present fabrication method.

3.5. Ratio of $(ZT)_\ell$ after annealing to that before annealing

Fig. 8 shows the distribution of the ratio of $(ZT)^a_\ell$ to $(ZT)^b_\ell$ for the *p*- and *n*-type specimens, where $(ZT)^a_\ell$ and $(ZT)^b_\ell$ are the local thermoelectric figure of merits after and before annealing, respectively. As listed in Table II, as a whole the annealing tended to enhance more significantly *ZT* of the *n*-type specimen than that of the *p*-type one. The spatial variation in $(ZT)^a_\ell/(ZT)^b_\ell$ of the *n*-type specimen was also much larger than that of the *p*-type one. In any case, the annealing has an effect to increase or decrease significantly $(ZT)_\ell$ from place to place. As described earlier, such a fluctuation in $(ZT)_\ell$ is considered to result from both only a slight deviation of the melt composition from the stoichiometry and only a little change in the degree of alignment of the *c*-planes of grains. It was thus found that the annealing effect on the thermoelectric figure of merit of bismuth-telluride bulk compounds is never uniform all over the specimen. If bismuth-telluride bulk compounds were prepared to have the same chemical composition and microstructure as those of the local region giving the largest $(ZT)_\ell$, therefore, an extremely high *ZT* value would be achieved even in bulk materials.

4. Summary

The *p*-type $(Bi_{0.25}Sb_{0.75})_2Te_3$ doped with 8 wt% excess Te alone and *n*-type $Bi_2(Te_{0.94}Se_{0.06})_3$ codoped with 0.017 wt% Te and 0.068 wt% I were grown by the Bridgman method and were cut into a parallele- piped of 5 × 5 × 15 mm^3, where the length of 15 mm is parallel to the freezing direction. Their local Seebeck coefficient α_ℓ and local electrical resistivity ρ_ℓ were measured at a scan step of 1 mm along the freezing direction of the specimen, before and after annealing at 673 K for 2 h in vacuum. The specimen is mounted on an *X*-*Y* stage and two probes are set at an interval of 1 mm. The local thermal conductivity κ_ℓ was calculated from ρ_ℓ using the relation between κ and ρ obtained macro-scopically for a series of bismuth-telluride compounds. α_ℓ ρ_ℓ and κ_ℓ before and after annealing changed from place to place, so that the annealing effect on $(ZT)_\ell$ is never uniform all over the specimen. Such a spatial variation in $(ZT)_\ell$ is considered to result from both only a slight deviation of the melt composition from the stoichiometry and only a little change in the degree of alignment of the *c* plane of grains. The maximum $(ZT)_\ell$ of the as-grown *p*- and *n*-type specimens reached surprisingly great values of 1.88 and 1.59, respectively, which correspond to about twice as large as those observed macroscopically by the conventional Seebeck coefficient apparatus. Probably the present maximum $(ZT)_\ell$ would be an upper limit of *ZT* for the *p*- and *n*-type bismuth-telluride bulk compounds. When bismuth-telluride bulk compounds were prepared to have the same chemical composition and microstructure as those of the local region giving the largest $(ZT)_\ell$ therefore, it is expected that *ZT* values of bulk materials approach considerably those of superlattice devices.

Acknowledgments

The authors would like to thank Mr. K. Satou for useful discussion and valuable technical support.

References

1. H. J. GOLDSMID, "Thermoelectric Refrigeration" (Plenum: NewYork, 1964).
2. O. YAMASHITA and S. TOMIYOSHI, *Jpn. J. Appl. Phys.* **42** (2003) 492.
3. O. YAMASHITA, S. TOMIYOSHI and K. MAKITA, *J. Appl. Phys.* **93** (2003) 368.
4. W. M. YIM and F. D. ROSI, *Solid State Electron.* **15** (1972) 1121.
5. L. D. IVANOVA, S. A. BROVIKOVA, H. SUSSMANN and P. REINSHAUS, *Inorg. Mater.* **31** (1995) 682.
6. H. P. HA, Y. W. CHO, J. Y. BYUN and J. D. SHIM, in Proceedings of the 12th International Conference on Thermoelectrics, Yokohama, Japan, 1993, p.105.
7. H. KAIBE, M. SAKATA, Y. ISODA and I. NISHIDA, *J. Jpn. Inst. Metals* **53** (1989) 958.

8. D.-B. HYUN, J.-S. HWANG, J.-D. SHIM and T. S. OH, *J. Mater. Sci.* **36** (2001) 1285.
9. J. SEO, K. PARK, D. LEE and C. LEE, *Scripta Mater.* **38** (1998) 477.
10. O. YAMASHITA, K. SATOU, H. ODAHARA and S. TOMIYOSHI, *J. Phys. Chem. Solids.* (in press)
11. M. NONNENMACHER and H. K. WICKRAMASINGHE, *Appl. Phys. Lett.* **61** (1992) 168.
12. C. C. WILLIAMS and H. K. WICKRAMASINGHE, *Nature* **344** (1990) 3177.
13. L. D. IVANOVA, Y. V. GRANATKINA, H. SUSSMANN and E. MULLER, *Inorg. Mater.* **29** (1993) 969.
14. H. SÜSSMANN, M. BOHM and P. REINHAUS, in Proceedings of the 12th International Conference on Thermoelectrics, Yokohama, Japan, 1993, p. 86.
15. M. TAKEDA, M. KURAMITSU and M. YOSHIO, *Thin Solid Films* **461** (2004) 179.
16. A. YAMAMOTO, D. KUKURUZNYAK, P. AHMER, T. CHIKYOW and F. S. OHUCHI, *Mater. Res. Soc. Proc.* **804** (2004) 3.
17. L. D. HICKS and M. S. DRESSELHAUS, *Phys. Rev. B* **47** (1993) 12727.
18. L. D. HICKS, T. C. HARMAN and M. S. DRESSELHAUS, *Appl. Phys. Lett.* **63** (1993) 3230.
19. L. D. HICKS and M. S. DRESSELHAUS, *Phys. Rev. B* **47** (1993) 16631.
20. R. VENENKATASUBRAMANIAN, E. SIIVOLA, T. COLPITTS and B. O'QUINN, *Nature* **413** (2001) 597.
21. L. D. IVANOVA, Y. U. V. GRANATKINA, N. V. POLIKARPOVA and E. I. SMIRNOVA, *Inorg. Mater.* **33** (1997) 558.
22. O. YAMASHITA and S. SUGIHARA, *J. Mater. Sci.* (in press).
23. I. TERAMOTO and S. TAKAYANAGI, *J. Phys. Chem. Solids* **19** (1961) 124.

Received 27 April 2004
and accepted 12 May 2005